Design and Preliminary Implementation of an N × N Diffractive All-Optical Fiber Optic Switch

Brittany Lynn, Pierre-Alexandre Blanche, Alexander Miles, John Wissinger, Daniel Carothers, Lloyd LaComb Jr., Robert A. Norwood, *Member, IEEE*, and Nasser Peyghambarian

***Abstract*—We have demonstrated a diffraction-based nonblocking, scalable N × N optical switch employing a digital micromirror display (DMD) with 12 μs switching speed, performing 100 times faster than the currently available technology. The distributed nature of diffraction makes this switch more robust than one-to-one reflective systems where a single mirror failure incapacitates an entire connection. We thereby address a key bottleneck in data centers and optical aggregation networks by decreasing circuit-switching speed and allowing for facile port count scalability.**

***Index Terms*—Digital micromirror device (DMD), free-space optical switch, optical crossconnect, optical switch, reconfigurable hologram, spatial light modulator (SLM), storage area networks (SANs).**

I. Introduction

TELECOMMUNICATIONS networking is a constantly evolving field in which the technology must continue to progress in order to keep pace with the demand of rising traffic volumes. Increasing network flexibility is one of the responses to this struggle, with dynamic network optical systems leading the way as a solution, allowing light path provisioning to distribute bandwidth on an as-needed basis [1]. Historically, systems required technician involvement to reprovision these paths but more recent implementations are moving toward algorithm-controlled, remote subsystems with reconfiguration times becoming a new bottleneck. Time spent reconfiguring a switch is time that the circuit is nontransmitting, placing stringent speed requirements on emerging optical switching technologies. The main benefits of using optical switches are that they are protocol and bit-rate independent, alleviating the requirement for frequent upgrades in response to changing network fabrics and increasing data rates. Additionally, the light-path redirection often occurs in free space, allowing modular designs to be scaled up to higher port count devices [2]. Three main drawbacks to current implementations are the requirement of manual manipulation, single point failure mechanisms, and speeds that fall short of meeting submillisecond application requirements.

A variety of optical switches based on an array of beam redirection devices have been developed to address these points, though none have succeeded across the board. The 3-D microelectromechanical system (MEMS) devices use two opposing arrays of small gimbaled mirrors to steer the light from one fiber to another in an analog steering manner. One commercially available system utilizing a 3-D MEMS design specifies a port count of 320 × 320, typical insertion loss of 2.0 dB and switching time of 25 ms [3]. The majority of the time required for switching in these 3-D-MEMS systems comes from the feedback loop required for precise angular positioning of the mirror. This mode of positioning also requires a constant voltage to be applied in order to maintain the mirror position. Liquid crystal display (LCD) spatial light modulators (SLMs) are another avenue for light-path modulation and use the orientation of high aspect ratio molecules in response to an applied voltage to impart birefringence and rotate incident polarization [4]. A 6 × 6 multimode ribbon fiber design has recently been described using a custom molecule-based phase SLM which when used in conjunction with a series of linear polarizers, functions as an addressable switch, either passing or blocking beams incident on subsections of the SLM. While the switch exhibits 1 μs switching time, it also has a loss of 20.5 dB, 11.5 dB of which is inherent in the fan-out and polarizer/SLM design [5]. Other systems use an SLM in reflection as an updatable holographic element, and act as one to many multicasting switches, but lack the ability to switch between multiple input ports [6]–[8]. Since these SLM-based systems use polarization as the switching mechanism, throughput can also be extremely sensitive to variations in signal polarization, which is undesirable for many applications.

Here, we describe an N × N free space holographic optical switch requiring no manual manipulation, exhibiting switching speeds less than 12 μs and negligible performance impact due to mirror failure. Also discussed is the preliminary implementation of a 9 × 9 system utilizing a digital micromirror device (DMD) acting as the redirection mechanism. The DMD consists of a 2-D array of 13.68 μm sized mirrors and is a binary device, resulting in two discrete addressable mirror positions with which to display a binary amplitude computer generated hologram. Unlike 3-D-MEMS, operation does not require a feedback positioning loop, instead relying on precisely located physical stops corresponding to the two mirror states. Once positioned, the

Manuscript received May 31, 2013; revised August 20, 2013; accepted August 28, 2013. Date of publication September 4, 2013; date of current version November 27, 2013. This work was supported by CIAN NSF ERC under Grant #EEC-0812072 and The University of Arizona Tech Launch Arizona POC Program.

B. Lynn, P.-A. Blanche, A. Miles, J. Wissinger, L. LaComb Jr., R. A. Norwood, and N. Peyghambarian are with the College of Optical Sciences, University of Arizona, Tucson, AZ 85721 USA (e-mail: blynn@optics.arizona.edu; pablanche@optics.arizona.edu; alexanderashtonmiles@gmail.com; jwissinger@optics.arizona.edu; llacomb@optics.arizona.edu; rnorwood@optics.arizona.edu; npp@u.arizona.edu).

D. Carothers is with Texas Instruments, Inc., Tucson, AZ 85711 USA (e-mail: dcarothers@optics.arizona.edu)

Color versions of one or more of the figures in this paper are available online at http://ieeexplore.ieee.org.

Digital Object Identifier 10.1109/JLT.2013.2280431

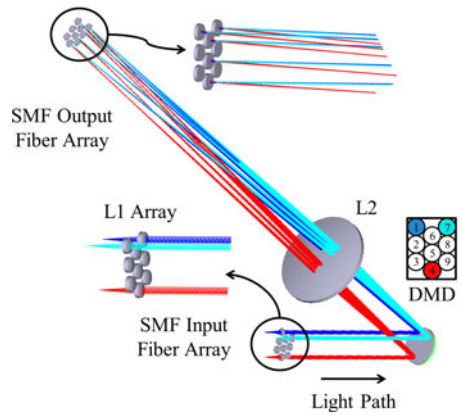

Fig. 1. Optical layout of the 9 × 9 holographic optical switch. Colors represent paths originating from different input ports.

voltage requirement to maintain the mirror setting is constant and does not need continual monitoring and update. In combination with the smaller mirrors, this results in a device that can switch orders of magnitude faster than a 3-D-MEMS device and requires no voltage adjustments while in a constant state. In addition, since the DMD operation is based on a reflection grating as its means of modulation, the system exhibits minimal polarization dependent loss (PDL). Employing diffraction as the beam direction mechanism gives us the freedom to implement a variety of ancillary features into the switch system, such as dynamically provisioning a pick-off beam for signal monitoring purposes, simultaneously sending data to more than one output for multicasting applications, and integrated variable attenuation control.

II. Switch Design

A. Switch Operation

The primary goal of this study is to create a proof of concept system by demonstrating the technology required for integration into a large scale reconfigurable N × N free space holographic optical switch that is insensitive to input polarization and wavelength. Our initial effort focused on the design and preliminary implementation of a dynamically updatable nine input port to nine output port switch. The development focused on incorporating a simple design, single mode fiber interfaces, and the ability to operate at any wavelength within the C-band (1530–1565 nm).

As shown in Fig. 1, the switch takes the beams from the input fiber array and collimates them at L1, where a series of 4 mm diameter, 12 mm focal length lenses are located. The lenses are AR coated to reduce reflection loss at 1550 nm. The beams are incident on individual subsets of the DMD (labeled 1–9 corresponding to the input fibers), each one displaying a hologram to diffract the beam to the correct output fiber. In order to switch from one output fiber to another, a new hologram is loaded onto that subset of the DMD and the beam is redirected accordingly. The Fourier lens, a 250 mm focal length lens labeled L2 in the figure, images the angular spectrum imparted by the hologram into discrete points at the back focal plane with magnification determined by the focal length of the lens. This switch is nonblocking, or one in which any connection can be established without affecting the existing connections. The model shows that the physical dimensions are compatible with standard 19 in × 22 in rack mount hardware.

B. DMD

The Texas Instruments DLP7000 used in the proof-of-principle switch has an array of 1024 × 768 mirrors, each one 13.68 μm × 13.68 μm in size with a fill factor of 92%. The mirrors can be oriented in two distinct positions, + 12° and −12° relative to the plane of the DMD, enabling its use as a binary amplitude grating by directing the reflection from one of the pixel states into the imaging system and the "dark" pixel illumination onto a beam dump. Our specific DMD has been manufactured with mirror and glass coatings optimized to function across the C-band [9]. Vibration and shock testing of DMD devices have demonstrated their robustness to a variety of environmental strains without significant physical or functional degradation. Reliability studies have shown lifetimes exceeding 10^{12} mirror cycles and 10^4 operating hours at high switching rates [10]. Operating temperatures for this mirror device range between 10 °C and 60 °C, enabling its use in a variety of network fabrics, from routing centers to high temperature data center rack environments [9].

In order to switch an input signal from one output port to another, the subset of pixels on the DMD that are devoted to that specific input port are reset independently from the rest of the mirrors, resulting in no loss of signal from other input ports. Mirror reset is a two-step process, first loading the new bit data onto the underlying CMOS memory, and then, updating the mirror positions by sending a reset pulse to the mirrors. This bit-data consists of a precalculated and optimized binary hologram stored in a look-up table, eliminating the need for on-the-fly computations. Upon receiving the reset pulse, switching speed for this unit is based on the loss-of-light time, which is the sum of the time it takes for the mirror to physically change position and the time it takes for the mirror to settle, resulting in an overall single-mode fiber switch time of 11.51 μs [11].

One of the benefits in using this device is its extremely low sensitivity to the polarization of a signal beam, with maximum PDL of 0.14 dB. This is in contrast to phase-based switching systems such as the ribbon fiber design previously mentioned which are optimized for a single polarization state and require cumbersome polarization diversity schemes [5]. An additional benefit to the holographic design of this switch is that performance does not depend critically on the functionality of a single mirror. An analysis of the effect of mirror failure on the insertion loss of this diffraction-based switch shows that a loss penalty over 0.2 dB requires the failure of more than 800 pixels per port. The results are shown in Fig. 2 for a variety of output port locations. This is in contrast to 3-D-MEMS-based devices where all of the power from each port is reflected from a single mirror at each MEMS device, leading to the complete loss of a port upon mirror failure. Single mirror reflection imposes an additional restriction on 3-D-MEMS devices in the form of

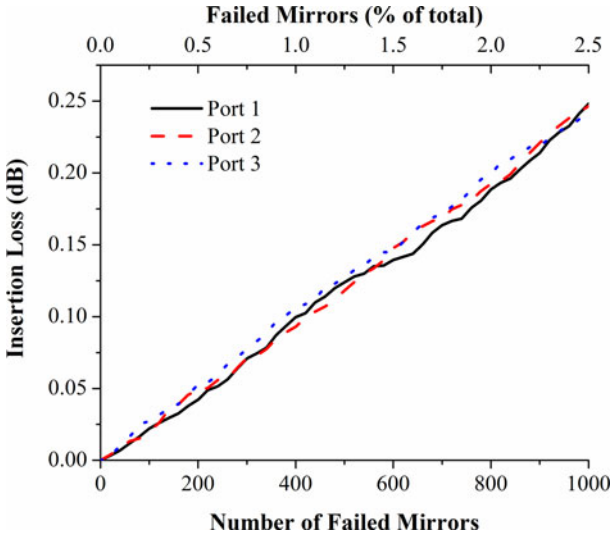

Fig. 2. Analysis of insertion loss due to randomized mirror failure for three output port locations.

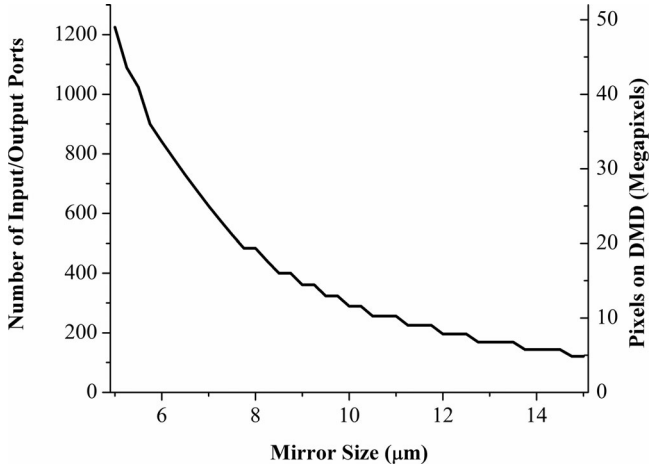

Fig. 3. Scalability study of the DMD-based switch. The analysis takes into account the extent of the DMD and the numerical aperture of the single mode fiber.

input power limitations. Since the power from a single beam is incident on an area averaging 0.3 mm^2, the total power per fiber is restricted to a few milliwatts. In our system, the flux from one fiber is spread over an area of 5.8 mm^2 and with a substrate optimized to handle high power display illumination; operating thresholds are well into the watt per fiber range. This opens the door to optical preamplification, if required, and high power implementations.

C. Hologram Design

An electromagnetic field incident on a periodically patterned surface behaves in a very predictable and reproducible manner, diffracting in a pattern related to that of the structure through the scalar diffraction theory [12]. This relation allows us to back-calculate the required diffraction pattern from the desired image plane structure by performing a series of scaled Fourier transforms. The resulting diffraction pattern generally consists of a superposition of an infinite number of frequencies containing continuously varying amplitude and phase information.

As a holographic element, the DMD allows us to access two states with which to implement a binary amplitude grating. The mirrors in the "ON" position correspond to the transmitted light in the amplitude structure while the mirrors in the "OFF" position correspond to the absorbed light. In conforming the mathematically obtained diffraction pattern to this binary amplitude-only device, we discard the phase information, binarize the amplitude information and discretize the spatial profile of the pattern to correspond to the DMD pixel size and spacing.

Discretization of the spatial profile of the pattern confines us to a specific set of system-dependent spatial frequencies which can be combined to approximate the desired frequency. The combination of frequencies in this implementation takes the form of a linear superposition of available frequencies where various combinations can be used to approximate the same field. To converge on the best superposition geared toward reduction of crosstalk and optimized output uniformity, we implemented the output–output algorithm kernel variation of the standard Gerchberg–Saxton iterative Fourier transform algorithm (IFTA) [13], [14]. This algorithm iterates through discrete Fourier transform calculations while adjusting the previous solution in an attempt to decrease the crosstalk error function. Implementation of this algorithm allowed us to minimize crosstalk between channels to below the noise floor of our measurement devices resulting in an isolation figure greater than 40 dB. An analysis of the beam intensity as an input beam is directed to different locations across the output plane was performed, resulting in a maximum variation of 0.3 dB observed across all possible output fiber locations. Uniformity on this scale indicates that this device would be able to support the transition to increased port counts and fiber densities. Using this algorithm, we can easily incorporate additional features into the switch such as diverting a small percentage of the signal to a detector for in-situ monitoring or even integrating a variable attenuation function for signal balancing.

Binarization of the amplitude-only pattern inherently limits the maximum energy that can be diffracted to a single location to $\sim$10%, resulting in multiple diffracted orders (or mirror images) to appear in the image plane in addition to the undiffracted beam (0 order) [12]. As the -1 diffracted order is a mirror image of the $+1$ order (about the zeroth order), this restricts the viable switching space to only one half of the accessible area within the switching region. Any fiber bundle that is oriented symmetrically about the zeroth order will exhibit significant crosstalk due to injection of the mirror image into another output port [8]. Another image artifact is caused by the less than 100% fill factor of the DMD, creating an additional repeating structure in the plane of the diffraction. This underlying periodic structure is of a similar frequency to the highest frequency accessible on the DMD, causing the unwanted features to be concentrated outside our region of interest.

Free-space optical switching and the holographic implementation of the DMD enable scaling of the system to port counts in the hundreds. Fig. 3 shows a scalability study performed on this switch with respect to the size of the pixels and the

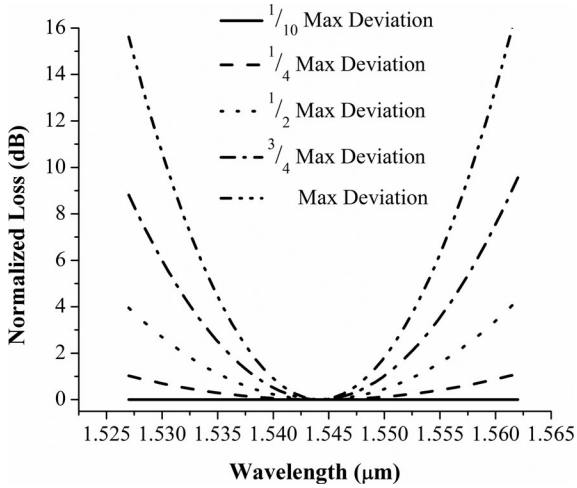

Fig. 4. Analysis of single mode fiber coupling loss as a function of signal wavelength across the output plane (normalized to the lowest loss case). Max deviation refers to the farthest distance the incoming beam can be deflected. Increased deviation corresponds to higher spatial frequencies displayed on the DMD.

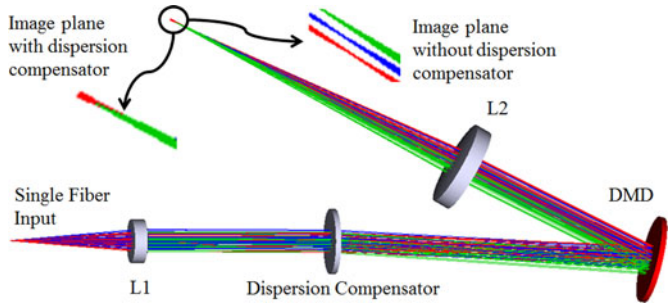

Fig. 5. Single channel model illustrating an exaggerated case of diffraction-based chromatic dispersion and its reduction by implementing a dispersion compensating grating. Colors represent various wavelengths within the C-band. Note the spatially separated focal points of the different wavelengths in the uncompensated case.

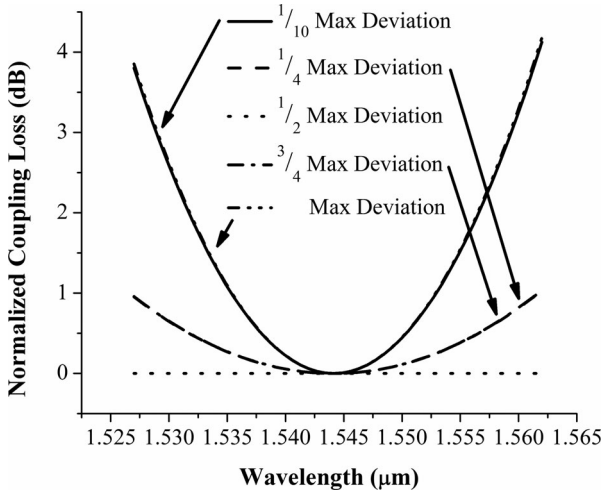

Fig. 6. Analysis of the single mode fiber coupling loss as a function of signal wavelength across the output plane after implementation of the dispersion compensator normalized to the lowest loss case. The throughput at the edges of the wavelength range is increased by a factor of 16.

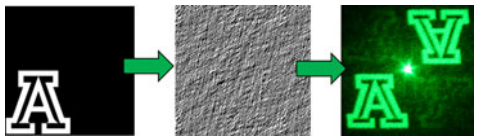

Fig. 7. Example schematic of hologram calculation and implementation using the DMD and coherent illumination.

corresponding DMD size. Moving to smaller pixels on the DMD increases the maximum angular deviation ($\theta_{\max}$) of the beam, as it is related through $\sin\theta_{\max} = \lambda/(2 * \text{pixel size})$. The larger the angular deviation we can achieve, the larger the space that can be accessed in the output plane. Each input port beam requires an array of DMD pixels on the order of 200 × 200. This size is defined by the inverse relation between the number of grating periods covered by the beam and the focal spot size required for coupling into the output fiber. A direct correlation exists between the number of input ports and the necessary pixel count. The analysis was performed based on a square grid of fibers at the output plane with center to center distance equal to the diameter of the fiber cladding and a maximum acceptance angle based on the numerical aperture for single mode fibers of 0.14. These results indicate that with the current pixel size of 13.68 μm, we can switch from any one of 144 input fibers to any one of 144 output fibers. Considering that DMD displays currently exist with over 2 Megapixels each, tiling only three displays would allow us to create a 144 × 144 optical switch.

D. Single Mode Fiber Coupling

The Fourier lens (L2) in the system design shown in Fig. 1, acts as an optical Fourier transform mechanism. This lens takes the frequency spectrum that results after diffraction from the DMD and forms it into an image at the rear focal plane of the lens. This spatial distribution of points in image space is geometrically related to the focal length of the lens, the wavelength of the illumination and the spatial frequencies displayed on the DMD. The physical extent of the point is governed by Gaussian beam propagation and depends on the collimated size of the beam and the focal length of the lens. In our case, the imaged point is around 16 times larger than the fiber diameter, causing substantial coupling loss in the current design expected to reach around 25 dB. The long focal length was needed to reach the correct image size while keeping the signal beams within the acceptance angle of the fiber, requiring a tradeoff between system NA and beam waist diameter. In future iterations, the output fibers will be mounted with decreased spacing, allowing the use of a shorter focal length lens, in turn increasing the fiber coupling efficiency to within standard device single mode coupling efficiencies (∼1 dB or so).

One of the application specific parameters that will affect coupling efficiency is the wavelength range that is contained within the input signal. The relationship among the wavelength (λ), grating frequency on the DMD (ξ), and the angles of incidence and diffraction (θ_I and θ_D, respectively) is given by $\lambda\xi = \sin(\theta_D) - \sin(\theta_I)$. Since the angle of diffraction is dependent on the illumination wavelength, the image location in the output plane is also dependent on the wavelength, shifting

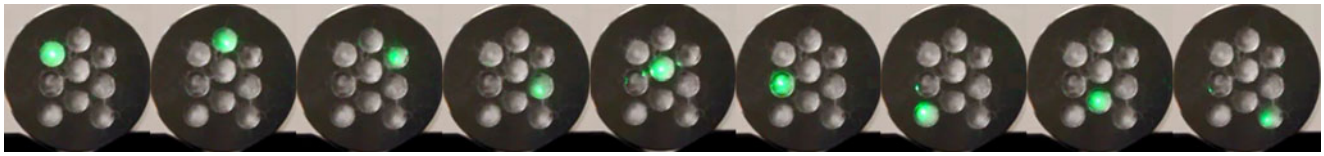

Fig. 8. Images showing the results of switching from a single input port to all output ports in sequence.

with a magnitude that is related to the focal length of the lens. This shift can be corrected in a system with a small band of wavelengths being transmitted by adjusting the diffraction pattern on the DMD, but in implementations that transmit across the entire C-band, correcting one wavelength will exacerbate the effect for another. Fig. 4 shows an analysis of the current implementation and the effect that wavelength has not only on the coupling loss but also on the port location, as ports farther from the center require larger diffraction angles, increasing the wavelength dependence.

In order to mitigate wavelength dependent coupling loss, we have designed a compensating grating which imparts a wavelength dependent angular deviation to the incident beam, deflecting longer wavelengths more strongly. These wavelengths now have various angles of incidence upon the DMD, with the longer wavelengths having a smaller angle of incidence than shorter wavelengths, and therefore, are deflected less than those with larger angles of incidence. This balance between wavelength and angularly dependent diffraction causes the various wavelengths to be collinear after the DMD and have the ability to be focused to a single output port location. Fig. 5 illustrates both the case with and without the dispersion compensator. The compensator is designed to flatten the wavelength dependent loss at a location central to the bundle in order to reduce the magnitude of the effect across the entire range of output locations as seen in Fig. 6.

III. Implementation at 532 nm

We implemented a 9×9 switch at 532 nm as a proof of the concept system in order to validate the functionality of the basic design and to ensure that the models accurately predicted the behavior and performance of diffraction using the DMD. Except for the fiber mounts, all of the components used in the design and implementation of this system were commercially available off-the-shelf parts including mounting and fiber aligning equipment. One benefit of testing at a visible wavelength was the ability to manipulate individual components and map out the alignment tolerances required for optimal performance using visual feedback. The initial test was of the IFTA and its ability to calculate a diffraction pattern of an arbitrary image, optimizing the uniformity of the image as well as reducing spurious features that could cause crosstalk in the output plane. Fig. 7 shows an example image, the calculated diffraction pattern, and the diffracted image upon illumination with coherent light. The bright point in the center of the diffracted image is the zeroth order beam and to either side of that can be seen the $+1$ and -1 diffracted orders, each with the expected uniformity. Next, we calculated the sequence of diffraction patterns corresponding to the various output port locations for the mount configuration. The output plane mount is a mirror image of the input plane and by loading the precalculated pattern and resetting the mirror states on the DMD, we were able to switch between all output ports as seen in Fig. 8. We showed sufficient control of point imaging to accurately locate the center of each output fiber location.

IV. Future Directions Considerations

The modeling and preliminary implementation discussed in this paper indicate that the holographic switch concept using a DMD is promising. The next step is the implementation at telecommunication wavelengths and system performance characterization such as insertion loss, crosstalk, port uniformity, and bit error rate testing.

One of the main contributors to loss that this switch will suffer from in the current design is the low diffraction efficiency ($\sim$10%) of the binary amplitude grating displayed by the DMD. This value is restricted by the physics of diffraction from a binary amplitude absorption/reflection grating. Under development are a variety of high-speed digital phase systems with a significant number of bit levels. These devices impart variable phase by shifting mirrors in a direction perpendicular to the plane of the device by fractions of the design wavelength, creating a multistep phase grating. A multistep phase micromirror device has the ability to approach 100% diffraction efficiency as the number of discretely addressable levels nears 10 to 20 but even with four phase levels the diffraction efficiency jumps above 80% [12]. In contrast to SLM type modulators, this multiphase micromirror device is able to retain the high switching speeds desired in this application. Implementation of this future type of modulator would minimize the losses of the switch due to diffraction, allowing us to implement other design adjustments to further increase switch throughput. One such alternative is to use two modulators in series to diffract the beams, correcting the out-coupling angle and wavelength dependence in a symmetric type system.

V. Conclusion

We have designed and implemented a 9×9 nonblocking switch at 532 nm as a proof-of-concept device on the way to full 9×9 capability in the C-band. The loss-of-light time for the DMD technology is less than 12 μs. The holographic implementation of the DMD provides a great degree of flexibility, allowing the creation of arbitrary switching patterns, including pick-off beams for *in-situ* monitoring and variable attenuation functionalities.

ACKNOWLEDGMENT

The authors would like to acknowledge Texas Instruments for the donation of the DMD and development package.

REFERENCES

[1] A. A. M. Saleh and J. M. Simmons, "All-optical networking—Evolution, benefits, challenges, and future vision," *Proc. IEEE*, vol. 100, no. 10, pp. 1105–1117, May 2012.

[2] G. I. Papadimitriou, C. Papazoglou, and A. S. Pomportsis, "Optical switching: Switch fabrics, techniques, and architectures," *J. Lightw. Technol.*, vol. 21, no. 2, pp. 384–405, Feb. 2003.

[3] "S320 photonic switch," Callient Technologies, Inc., Goleta, CA, USA, S320 datasheet, 2013.

[4] C. V. Garcia, I. P. Garcilopez, P. C. Lallana, B. Vinouze, and B. Fracasso, "Liquid crystal optical switches," in *Optical Switches: Materials and Design*, B. Li and S. J. Chua, Eds. Cambridge, U.K.: Woodhead Publishing, 2010, pp. 206–240.

[5] H. Chou, F. Zhang, T. D. Wilkinson, N. Collings, and W. A. Crossland, "Implementation of a 6 × 6 free-space optical fiber ribbon switch for storage area networks," *J. Lightw. Technol.*, vol. 30, no. 11, pp. 1719–1725, Jun. 2012.

[6] B. Robertson, Z. Zhang, H. Yang, M. M. Redmond, N. Collings, J. Liu, R. Lin, A. M. Jeziorska-Chapman, J. R. Moore, W. A. Crossland, and D. P. Chu, "Application of the fractional Fourier transform to the design of LCOS based optical interconnects and fiber switches," *Appl. Opt.*, vol. 51, pp. 2212–2222, 2012.

[7] W. A. Crossland, I. G. Manolis, M. M. Redmond, K. L. Tan, T. D. Wilkinson, M. J. Holmes, T. R. Parker, H. H. Chu, J. Croucher, V. A. Handerek, S. T. Warr, B. Robertson, I. G. Bonas, R. Franklin, C. Stace, H. J. White, R. A. Woolley, and G. Henshall, "Holographic optical switching: The "ROSES" demonstrator," *J. Lightw. Technol.*, vol. 18, no. 12, pp. 1845–1854, Dec. 2000.

[8] C. Letort, B. Vinouze, and B. Fracasso, "Design and fabrication of a high-density 2D fiber array for holographic switching applications," *Opt. Eng.*, vol. 47, p. 045401, 2008.

[9] "DLP 0.7 XGA 2xLVDC type a DMD," Texas Instruments, Dallas, TX, USA, DLP 7000 datasheet, 2012.

[10] M. R. Douglass, "Lifetime estimates and unique failure mechanisms of the digital micromirror device (DMD)," in *Proc. 36th Annu. Int. Rel. Phys. Symp.*, 1998, pp. 9–16.

[11] N. Farrington, A. Forencich, S. Member, G. Porter, P. Sun, J. E. Ford, Y. Fainman, G. C. Papen, and A. Vahdat, "A multiport microsecond optical circuit switch for data center networking," *IEEE Photon. Technol. Lett.*, vol. 25, no. 16, pp. 1589–1592, Aug. 2013.

[12] H. Kogelnik, "Coupled wave theory for thick hologram gratings," *The Bell Syst. Tech. J.*, vol. 48, pp. 2909–2947, 1969.

[13] J. R. Fienup, "Iterative method applied to image reconstruction and to computer-generated holograms," *Opt. Eng.*, vol. 19, pp. 297–305, 1980.

[14] V. Kettunen, "Review of iterative Fourier-transform algorithms for beam shaping applications," *Opt. Eng.*, vol. 43, pp. 2549–2556, 2004.

Authors' biographies not available at the time of publication.